nature structural & molecular biology

Structural basis for midbody targeting of spastin by the ESCRT-III protein CHMP1B

Dong Yang[1], Neggy Rismanchi[2], Benoît Renvoisé[2], Jennifer Lippincott-Schwartz[3], Craig Blackstone[2] & James H Hurley[1]

The endosomal sorting complex required for transport (ESCRT) machinery, including ESCRT-III, localizes to the midbody and participates in the membrane-abscission step of cytokinesis. The ESCRT-III protein charged multivesicular body protein 1B (CHMP1B) is required for recruitment of the MIT domain–containing protein spastin, a microtubule-severing enzyme, to the midbody. The 2.5-Å structure of the C-terminal tail of CHMP1B with the MIT domain of spastin reveals a specific, high-affinity complex involving a noncanonical binding site between the first and third helices of the MIT domain. The structural interface is twice as large as that of the MIT domain of the VPS4–CHMP complex, consistent with the high affinity of the interaction. A series of unique hydrogen-bonding interactions and close packing of small side chains discriminate against the other ten human ESCRT-III subunits. Point mutants in the CHMP1B binding site of spastin block recruitment of spastin to the midbody and impair cytokinesis.

The ESCRT machinery is best known for its role in membrane-cleavage events during the inward budding of intralumenal vesicles into endosomes[1,2] and in the budding of enveloped viruses such as HIV-1 from the plasma membrane[3]. However, two key components of the ESCRT machinery, ESCRT-I and ALG-2–interacting protein X (ALIX), were recently found to localize to the midbody, where they carry out essential roles in membrane abscission during cell division[4,5].

Cytokinesis, the division of the cytoplasm, is the final step of the M phase of the cell cycle, and the key events in cytokinesis are coordinated by the microtubule-based central spindle[6]. Cytokinesis begins with the formation of the contractile ring, which drives the growth of the cleavage furrow. When the furrow extension ends, the contractile ring disassembles, and a structure known as the midbody remains as the final tether between the two daughter cells. The midbody consists of tightly packed microtubules and associated proteins. Much recent attention has centered on the recruitment of membrane-trafficking machinery to the midbody to carry out the cleavage of the membrane neck, a process known as abscission[4,5,7–9]. In addition to ESCRT-I and ALIX, ESCRT-III has emerged as an intriguing player in cytokinesis. ESCRT-III proteins form circular arrays[10] or tubes[11], which suggest a possible means for their putative membrane-scission activity[10]. In fact, ESCRT-III subunits that localize to midbodies and have been implicated in cytokinesis include CHMP2A, CHMP4A, CHMP5 (ref. 5) and CHMP3 (ref. 12). (Human ESCRT-III subunits and corresponding yeast orthologs are as follows: CHMP1, Did2; CHMP2, Vps2; CHMP3, Vps24; CHMP4, Snf7; CHMP5, Vps60; CHMP6, Vps20).

MIT (present in microtubule-interacting and trafficking molecules) domains are a divergent group of three-helix bundles that in many cases bind to C-terminal motifs in ESCRT-III proteins[13]. Indeed, the MIT domain of the AAA+ ATPase VPS4 binds to CHMP1B, and the structure of the complex has been determined[14]. CHMP1A, 1B, 2A and 2B constitute a subset of ESCRT-III proteins containing a 'MIT-interacting motif' (MIM) that binds to the VPS4 MIT domain[15]. VPS4 disassembles membrane-bound ESCRT-III aggregates, and the MIT domain–MIM interaction is the main mechanism by which VPS4 binds its substrate.

The N-terminal region of the microtubule-severing protein spastin, another AAA+ ATPase, also harbors a MIT domain that binds to the ESCRT-III protein CHMP1B[16]. Spastin is encoded by *SPG4*, which is mutated in the most common form of hereditary spastic paraplegia. The hereditary spastic paraplegias constitute a group of inherited neurological disorders characterized by progressive spasticity and weakness of the lower limbs due to a length-dependent axonopathy of upper motor neurons. Although nearly 40 distinct genetic loci have been described (*SPG1*–*SPG38*), up to 40% of the cases are caused by autosomal dominant *SPG4* mutations[17]. The C-terminal AAA+ ATPase domain of spastin forms a hexamer around a central pore, whereas the N-terminal regions project from the central core and bind to tubulin subunits[18]. Spastin orthologs are present in *Caenorhabditis elegans* and *Drosophila melanogaster*, and the protein is widely expressed in human tissues and cell types throughout the body. Although spastin has been implicated in cytoskeletal rearrangement and dynamics, its functional roles within the cell remain unclear.

[1]Laboratory of Molecular Biology, National Institute of Diabetes and Digestive and Kidney Diseases, [2]Cellular Neurology Unit, Neurogenetics Branch, National Institute of Neurological Disorders and Stroke and [3]Cell Biology and Metabolism Program, National Institute of Child Health and Human Development, National Institutes of Health, US Department of Health and Human Services, Bethesda, Maryland 20892, USA. Correspondence should be addressed to C.B. (blackstc@ninds.nih.gov) or J.H.H. (hurley@helix.nih.gov).

Received 12 June; accepted 10 October; published online 9 November 2008; doi:10.1038/nsmb.1512

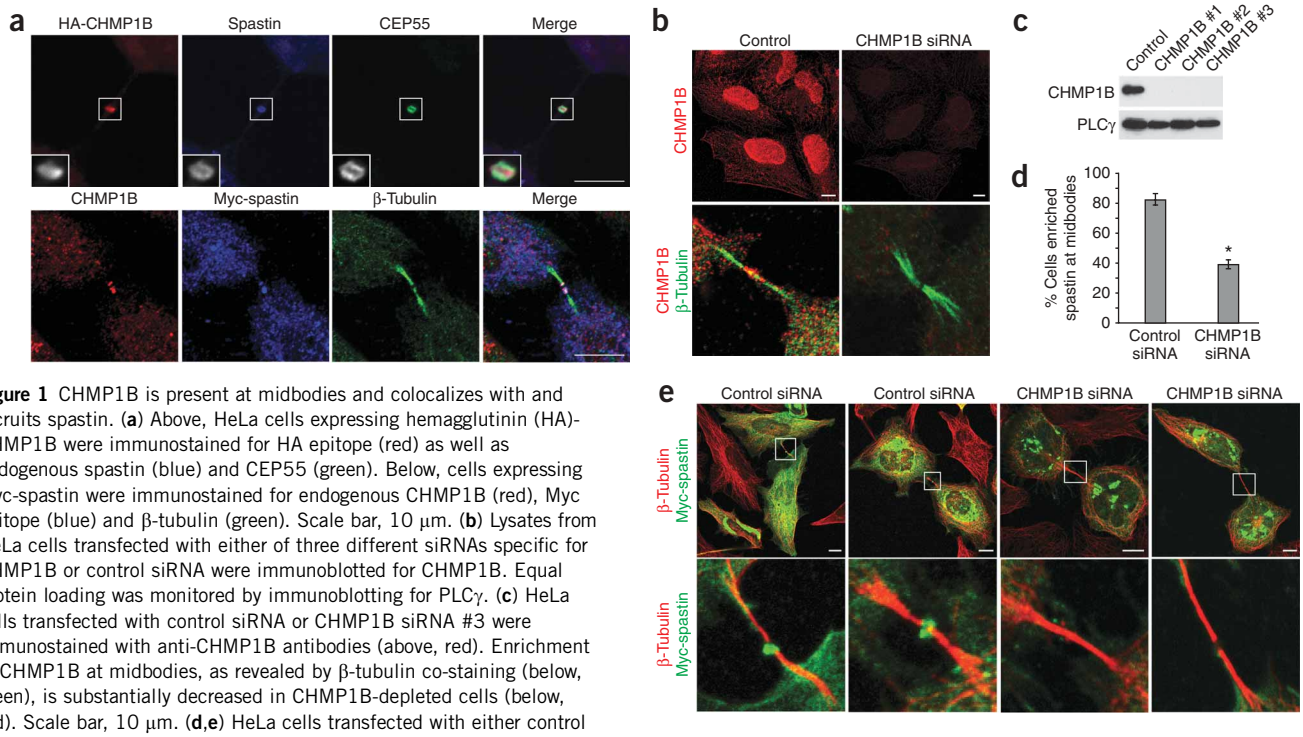

Figure 1 CHMP1B is present at midbodies and colocalizes with and recruits spastin. (**a**) Above, HeLa cells expressing hemagglutinin (HA)-CHMP1B were immunostained for HA epitope (red) as well as endogenous spastin (blue) and CEP55 (green). Below, cells expressing Myc-spastin were immunostained for endogenous CHMP1B (red), Myc epitope (blue) and β-tubulin (green). Scale bar, 10 μm. (**b**) Lysates from HeLa cells transfected with either of three different siRNAs specific for CHMP1B or control siRNA were immunoblotted for CHMP1B. Equal protein loading was monitored by immunoblotting for PLCγ. (**c**) HeLa cells transfected with control siRNA or CHMP1B siRNA #3 were immunostained with anti-CHMP1B antibodies (above, red). Enrichment of CHMP1B at midbodies, as revealed by β-tubulin co-staining (below, green), is substantially decreased in CHMP1B-depleted cells (below, red). Scale bar, 10 μm. (**d**,**e**) HeLa cells transfected with either control or CHMP1B siRNA were retransfected with Myc-spastin. (**d**) Quantification of spastin enrichment at midbodies in CHMP1B or control siRNA treated cells ($n = 3$; 100 cells per experiment; ± s.d.). * indicates $P < 0.001$. (**e**) Midbodies, as identified by β-tubulin staining (red), show a lack of spastin (green) enrichment in CHMP1B-depleted cells (right two panels) as compared with control cells (left two panels). The boxed area in the row above is enlarged below. Scale bar, 10 μm.

Spastin has been shown to localize prominently to the midbody[19]. In light of recent findings that ESCRT participates in membrane abscission in cytokinesis and that many ESCRT components localize to the midbody, the demonstrated midbody localization of spastin and the ability of spastin to bind to CHMP1B, we decided to explore whether CHMP1B and spastin might recruit or regulate one another at the midbody.

We found that CHMP1B and spastin colocalize at midbodies in dividing HeLa cells, and knockdown of CHMP1B reduced the amount of spastin at midbodies. Biochemical analysis showed that spastin interacted with CHMP1B with a higher affinity than other previously characterized MIT domain–ESCRT-III interactions. We went on to determine the crystal structure of the complex between the C-terminal ~40% of CHMP1B (CHMP1B-CTR) and the MIT domain of spastin and characterized their binding interaction. The structure manifested an interface nearly twice as large as the previously described MIT domain–ESCRT-III interactions and contained many hydrogen bonds, consistent with a highly specific mode of interaction. On the basis of the crystal structure, we engineered a mutant form of spastin incapable of binding to CHMP1B. This mutant spastin does not localize to midbodies. These results show that spastin and CHMP1B interact in a highly specific manner and that CHMP1B recruits spastin to the midbody, suggesting that spastin could have a role in cytokinesis.

RESULTS

Depletion of CHMP1B impairs spastin localization

Spastin localizes prominently to the midbody in dividing cells[19] (**Fig. 1a**), and we examined the localization of hemagglutinin-tagged CHMP1B as well as endogenous CHMP1B in HeLa cells (**Fig. 1**). Notably, CHMP1B was enriched at midbodies in dividing cells, where it colocalized prominently with endogenous and Myc-tagged spastin as well as endogenous centrosomal protein 55kDa (CEP55) (**Fig. 1a**) and CHMP5 (**Supplementary Fig. 1c** online). CHMP1B was also present diffusely throughout the cytoplasm and in the nucleus (**Fig. 1b**). In most cells, both spastin and CHMP1B appeared localized at the periphery of the Flemming body, as identified using phase-contrast imaging (**Fig. 1a**). Immunostaining also appeared centrally in some midbodies, particularly when proteins were overexpressed, but spastin and CHMP1B were consistently more enriched peripherally (data not shown). Together, these data support a more peripheral midbody localization for both CHMP1B and spastin, and this colocalization prefigured an important cellular context for the functional interaction of spastin and CHMP1B.

We investigated whether the CHMP1B-spastin interaction was important for protein targeting. After knocking down CHMP1B expression using small interfering RNA (siRNA), we found that nearly all CHMP1B staining was specifically depleted at the midbody and elsewhere throughout the cell, confirming the specificity of the antibody (**Fig. 1b**,**c**). In cells expressing Myc-spastin, CHMP1B depletion by siRNA resulted in the disappearance of Myc-spastin from the midbody in most cells (**Fig. 1d**,**e**). Spastin was present at midbodies in 82.3 ± 3.5% of control siRNA–treated cells, but in only 39.0 ± 2.7% of CHMP1B siRNA-treated cells (**Fig. 1d**), indicating that CHMP1B has a role in the recruitment of spastin to the midbody.

Recent studies have indicated that depletion of ESCRT-III proteins can alter midbody structure and morphology[20], and in fact we saw evidence of this in cells lacking CHMP1B. In some cases, the characteristic dark zones of the midbodies did not seem to be present (**Fig. 1e**). To establish that the lack of spastin at midbodies in CHMP1B siRNA–treated cells did not simply reflect loss of midbodies,

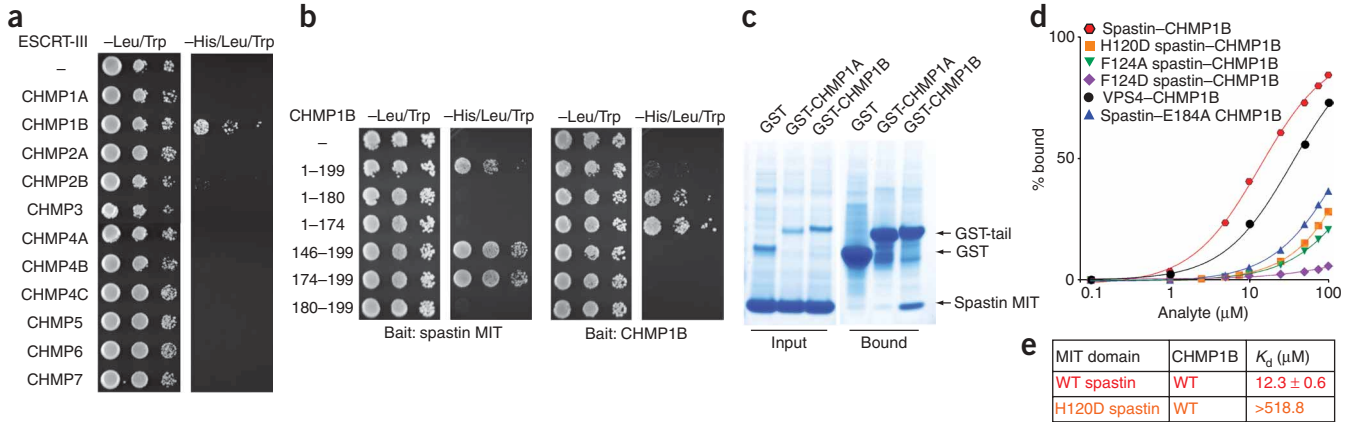

e

MIT domain	CHMP1B	K_d (μM)
WT spastin	WT	12.3 ± 0.6
H120D spastin	WT	>518.8
F124A spastin	WT	>281.8
F124D spastin	WT	ND
WT spastin	E184A	>152.3
VPS4	wt	33.3 ± 0.1

Figure 2 Spastin–CHMP1B interactions. (**a**) Yeast two-hybrid interactions between the spastin MIT domain bait and the indicated CHMP prey constructs were assayed using the *HIS3* reporter (sequential ten-fold yeast dilutions are shown). (**b**) Spastin MIT and CHMP1B baits were tested for yeast two-hybrid interactions as in **a** with the indicted CHMP1B prey constructs. (**c**) GST fusion of the CHMP1B-CTR, but not the CHMP1A-CTR, pulls down the spastin MIT domain *in vitro*. (**d**) SPR analysis of spastin and the VPS4A MIT domain binding to immobilized CHMP1B-CTR. The analyte is either the spastin or the VPS4A MIT domain, as indicated. (**e**) Tabulated binding constants (K_d) or their lower limits.

we depleted another midbody ESCRT-III subunit, CHMP5, using siRNA (**Supplementary Fig. 1**). In CHMP5-depleted cells, which showed similar effects on midbodies, spastin localized to midbodies in 73.7 ± 17.4% of cells, compared with 94.4 ± 3.0% in the control siRNA–treated cells ($P = 0.23$), indicating the specificity of CHMP1B among ESCRT-III subunits in spastin recruitment (**Supplementary Fig. 1a**,**b**). In fact, even the minimal decrease in spastin recruitment in CHMP5-depleted cells might be fully explained by the decreased presence of CHMP1B at midbodies in these cells (**Supplementary Fig. 1c**,**d**).

The spastin–CHMP1B interaction

To establish further the role of CHMP1B in recruitment of spastin to midbodies, we investigated the specificity of spastin interactions with ESCRT-III proteins, using yeast two-hybrid assays to study interactions of the spastin MIT domain with the 11 known human CHMP proteins. The MIT domain of spastin (residues 110–195) interacted robustly with CHMP1B (**Fig. 2a**) but not with any other CHMP proteins tested, including CHMP1A. The C terminus of CHMP1B (residues 174–199) was necessary and sufficient for this interaction (**Fig. 2b**). However, the number of CHMP1B residues required for the interaction was greater than that predicted from the published CHMP1B–VPS4 MIM interaction. Notably, C-terminal domains of CHMP proteins function as autoinhibitory switches[21–23], and indeed removal of the C-terminal spastin binding domain of CHMP1B markedly increased its ability to self-associate (**Fig. 2b**). To determine whether isolated C termini of other CHMPs might uncover weaker interactions with the spastin MIT domain, we tested all CHMP C termini against the spastin MIT domain in yeast two-hybrid tests. We found that CHMP1B interaction with spastin was highly specific regardless of whether it was assayed with the full-length proteins or the C-terminal tails (**Supplementary Fig. 2** online).

To corroborate the unique preference of the spastin MIT domain for CHMP1B as opposed to all other CHMP isoforms, we compared the binding of the purified C-terminal tails of CHMP1B and its closest homolog CHMP1A (**Fig. 2c**). Consistent with the yeast two-hybrid results, we observed no binding of the spastin MIT domain to the CHMP1A tail. We measured the affinity of the spastin MIT domain–CHMP1B interaction by surface plasmon resonance (SPR) and obtained a $K_d = 12$ μM, substantially higher than the 33 μM for the VPS4 MIT domain binding to CHMP1B[14] (**Fig. 2d**,**e**). Taken together, these results demonstrate that the spastin MIT domain is highly specific for interaction with CHMP1B and binds to it more tightly than occurs in other characterized MIT domain–ESCRT-III interactions.

Structure of the spastin–CHMP1B complex

To investigate the structural basis for this specificity, we determined the crystal structure of the spastin MIT domain bound to the CHMP1B-CTR refined at 2.5-Å resolution (**Fig. 3a** and **Supplementary Fig. 3** online). There are six copies of a 1:1 spastin MIT–CHMP1B-CTR complex in the asymmetric unit (**Supplementary Fig. 4** online). The C-terminal helix of CHMP1B, comprising residues 174–196, fills a 30-Å groove between helices α1 and α3 that runs the entire length of the spastin MIT domain (**Fig. 3a**,**b**). A second helical fragment from CHMP1B, spanning residues 148–163, was also visualized in the structure. This helix folds against the back side of the CHMP1B C-terminal helix (**Fig. 3a**) and has minimal contact with the MIT domain. The total surface area buried upon complex formation is 1,946 Å^2. Of this area, the C-terminal helix alone is responsible for the burial of 1,836 Å^2.

The C-terminal-most three turns of the CHMP1B C-terminal helix contain the MIM, the same region previously found to be responsible for binding to the MIT domain of VPS4. Leu188 and Leu192, the first two leucine residues of the MIM, are completely buried in hydrophobic pockets in the spastin MIT domain groove (**Fig. 3b**). The third leucine of the MIM, Leu195, is partially buried. Spastin residues Phe124, Leu127 and Ile131 of α1, and Met187 of α3, are the major hydrophobic residues in contact with the MIM leucine residues. The remaining leucine binding sites are contributed by aliphatic portions of polar side chains. The C-terminal half of the CHMP1B C-terminal helix makes just two polar contacts with the MIT domain: CHMP1B Arg191 makes a salt-bridge with spastin Glu135, whereas CHMP1B Ser189 forms a hydrogen bond with spastin Asn184 (**Fig. 3c**,**d**).

In contrast to the C-terminal half of the CHMP1B helix described above, the three turns of the N-terminal half lack large hydrophobic

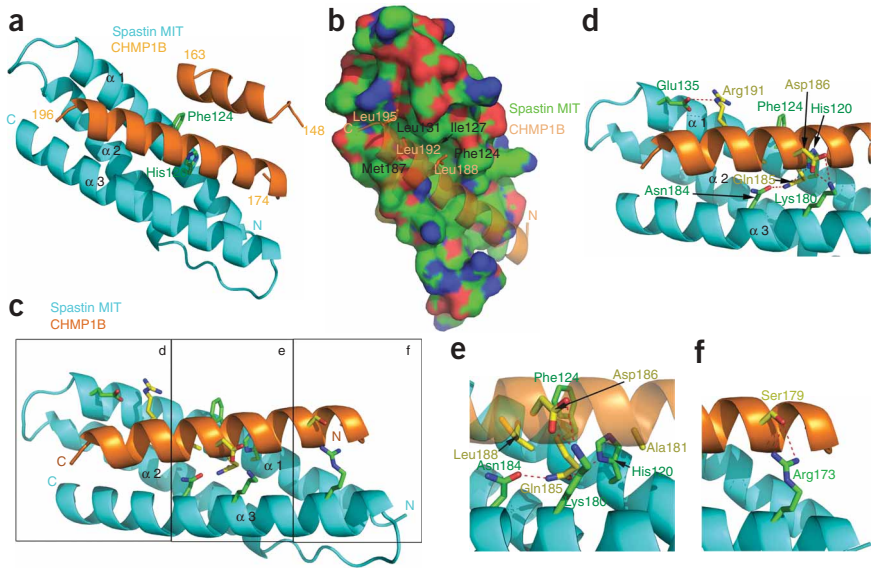

Figure 3 Structure of the spastin MIT domain–CHMP1B complex. (**a**) Overall structure of the MIT domain (blue) and CHMP1B (orange). (**b**) Key MIM leucine residues bind to hydrophobic pockets in the groove between α1 and α3 of the MIT domain. The spastin MIT domain surface is colored green for carbon atoms, red for oxygen and blue for nitrogen. Contiguous green regions indicate hydrophobic surfaces. (**c**) Overview of polar interactions between CHMP1B-CTR and the spastin MIT domain. (**d**–**f**) Details of interactions as seen in insets **d**–**f** within **c**.

side chains (**Fig. 3c**,**e**,**f**). The residues in this region diverge from the sequences of all other ESCRT-III proteins (**Fig. 4a**). Of the seven residues within this region that make direct contact with the spastin MIT domain, only one is identical in CHMP1A (**Fig. 4a**). These interactions include hydrogen bonds between CHMP1B Ser175 and Ser179 with spastin Arg173, CHMP1B Thr178 with spastin Arg117, and CHMP1B Asp186 with spastin Lys180 (**Fig. 3e**). CHMP1B Glu184 and Gln185 form a hydrogen-bond relay with spastin His120 and Asn184. Spastin His120 is sandwiched between the two CHMP1B side chains, whereas CHMP1B Gln184 is sandwiched between the two spastin side chains (**Fig. 3e**). Hydrophobic contacts are made between spastin and the small side chains of Val180, Ala181 and Ala183 (**Fig. 3e**,**f**). The restricted packing around these small side chains precludes the presence of any larger residues at these positions. As described below in more detail, mutation of small amino acids in this region to larger ones abrogates binding to spastin, but not VPS4 (**Fig. 4b**). The combination of hydrogen-bonding and steric-packing restrictions imposes strict constraints on the nature of sequences capable of binding to this half of the α1-α3 groove.

Specificity determinants

The spastin MIT domain binding site for CHMP1B lies between helices α1 and α3. This is in sharp and unexpected contrast to the Vps4 MIT domain, which uses a site between α2 and α3 to bind to MIMs (**Fig. 4c**). In a second major contrast, the spastin MIT–CHMP1B interface is nearly twice as extensive as the VPS4A MIT interface. The VPS4A–CHMP1A complex[14] buries 1,013 Å^2 of surface area, just half of the area buried in the spastin–CHMP1B complex. The C-terminal CHMP1B helix bound to spastin is twice as long as the CHMP1A helix bound to VPS4A, fully accounting for the difference in buried surface area.

To highlight the similarities and differences, we constructed a model for the CHMP1B–VPS4A MIT domain complex by overlaying the crystallized CHMP1B C-terminal helix with the CHMP1A MIM as seen in the solution structure of its complex with VPS4A (**Fig. 4c**). Despite the major differences in the location and extent of the binding site described above, all three key leucine residues of the CHMP1B helix bind to hydrophobic pockets on both of the MIT domains (**Fig. 4d**,**e**). The character of the pockets is similar, even though they are made up of completely different residues on two different faces of the MIT domain. Arg191, part of the MIM consensus, forms a salt bridge in both contexts, again with acidic residues in completely different positions on the MIT domain. Thus, the conserved MIM region is bifunctional in CHMP1B in that it binds to both VPS4 and spastin MIT domains. The dual function of the MIM leucine residues confers on CHMP1B its ability to bind to both spastin and VPS4, but not both at the same time. We tested this structural observation using an *in vitro* competition assay (**Fig. 4f**), and found that the spastin and VPS4 MIT domains compete for the same site, consistent with the overlapping binding site observed in the structures.

The unique determinants for spastin binding are almost all located in the N-terminal half of the CHMP1B helix. Within the N-terminal portion (residues 174–185), eight CHMP1B residues form hydrogen bonds or van der Waals interactions with the spastin MIT domain. Of these, only Ser179 is identical in CHMP1A. Of the remaining seven, several sequence differences in CHMP1A versus CHMP1B give rise to changes in charge, loss of hydrogen bonds and predicted steric clashes. For example, the tightly packed Thr178 and Ala181 in CHMP1B are replaced by the larger glutamic acid and valine residues in CHMP1A. Although none of these sequence changes between CHMP1A and 1B seem likely to completely abrogate binding on their own, in aggregate they explain how spastin discriminates against even the most closely related CHMP1B homologs, such as CHMP1A.

Mutational analysis of binding

Spastin Phe124 lies at the heart of the CHMP1B binding site and makes extensive contact with CHMP1B Leu188 and surrounding residues. The spastin mutations F124A and F124D drastically reduce the affinity of the complex as assessed by SPR, consistent with the structure. Mutation of two polar MIT domain residues tested, Arg117 and Arg173, produced either no effect on affinity or increased the affinity slightly (data not shown). Another polar mutation, H120D, sharply reduced binding by more than 40-fold (**Fig. 2d**,**e** and **Supplementary Fig. 5** online). On CHMP1B, mutation of a key polar residue interacting with spastin His120, E184A, decreased affinity by more than ten-fold by SPR (**Fig. 2d**,**e** and **Supplementary Fig. 5**).

Yeast two-hybrid studies corroborated these SPR data. Spastin$_{110–195}$-H120D F124D showed no detectable interaction with CHMP1B (**Supplementary Fig. 6** online). A triple mutant in which three of the CHMP1B-unique residues, Thr178, Ala181 and Glu184, were mutated to arginine, whose bulky side chains were expected to disrupt packing, completely abrogated binding (**Fig. 4b**). Even so, the same CHMP1B triple mutant still interacted robustly with the VPS4A MIT domain (residues 1–82; **Fig. 4b**), consistent with structural modeling showing

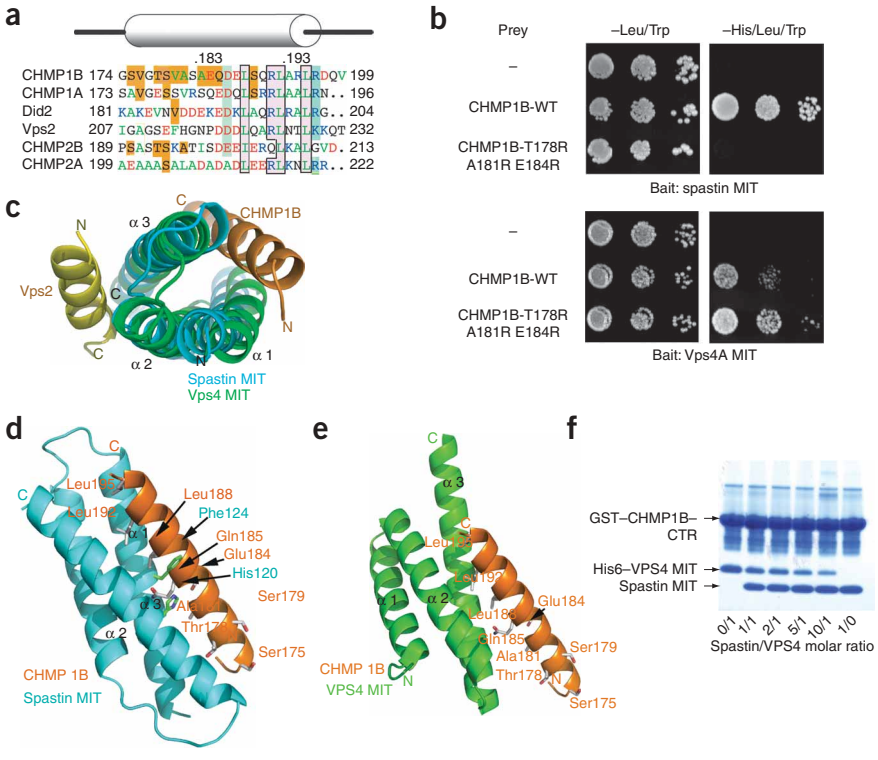

Figure 4 Overlapping specificity determinants in MIT domain recognition. (**a**) Structure-based sequence alignment of CHMP1B and other MIM-containing ESCRT-III proteins. Residues are boxed in gold for spastin MIT–specific contacts, green for VPS4 MIT–specific contacts and pink with black outlines for residues that make contacts with both MIT domains. Residue abbreviation typeface is colored according to residues properties: green, hydrophobic; red, negatively charged; and blue, positively charged. (**b**) Yeast two-hybrid analysis using the *HIS3* reporter (ten fold yeast dilutions are shown) investigating the indicated CHMP1B triple mutant that abolishes spastin MIT binding, but not VPS4A MIT binding. (**c**) The spastin MIT (blue)–CHMP1B (orange) complex is overlaid on the yeast Vps4 MIT (green)–Vps2 (yellow) complex using a structural alignment between the MIT domains to show that the CHMP1B and Vps2 bind to different sites on opposite faces of the MIT domain. (**d**,**e**) Side-by-side view of the spastin MIT–CHMP1B complex (**d**) and a docked model of the VPS4 MIT–CHMP1B complex (**e**), colored as in **c**. (**f**) The spastin MIT domain competes with the VPS4 MIT domain for binding to GST– CHMP1B-CTR *in vitro*. Molar ratios of these two MIT domains are shown below the figure. The concentration of the VPS4 MIT domain was held constant, whereas the concentration of the spastin MIT domain was varied.

a large gap between these residues and the MIT domain (**Fig. 4e**). Consistent with the structure, replacement of Leu188 and Leu192 with alanine eliminated the interaction of CHMP1B with both spastin and Vps4 MIT domains *in vitro* (**Supplementary Fig. 7** online).

Spastin MIT mutation impairs midbody localization

As spastin-H120D F124D does not interact with CHMP1B, we examined its distribution in HeLa cells. Whereas wild-type Myc-tagged spastin was enriched at midbodies as expected, Myc–spastin-H120D F124D was not detectable at midbodies in most cells. Wild-type Myc-spastin was present at midbodies in 88.4 ± 3.5% of transfected cells, whereas Myc–spastin-H120D F124D was present at midbodies in only 21.0 ± 7.9% of cells (**Fig. 5a**,**b**), consistent with a requirement for CHMP1B interaction for midbody localization of spastin. Cells overexpressing Myc–spastin-H120D F124D also showed impaired cytokinesis (**Fig. 5c**,**d**), as manifested by persistent linkages among cells, whereas no such effect was observed in cells overexpressing wild-type Myc-spastin. In fact, 31.3 ± 9.3% of cells expressing Myc–spastin-H120D F124D showed evidence of interconnections, as compared to only 7.7 ± 5.0% of cells transfected with wild-type Myc-spastin.

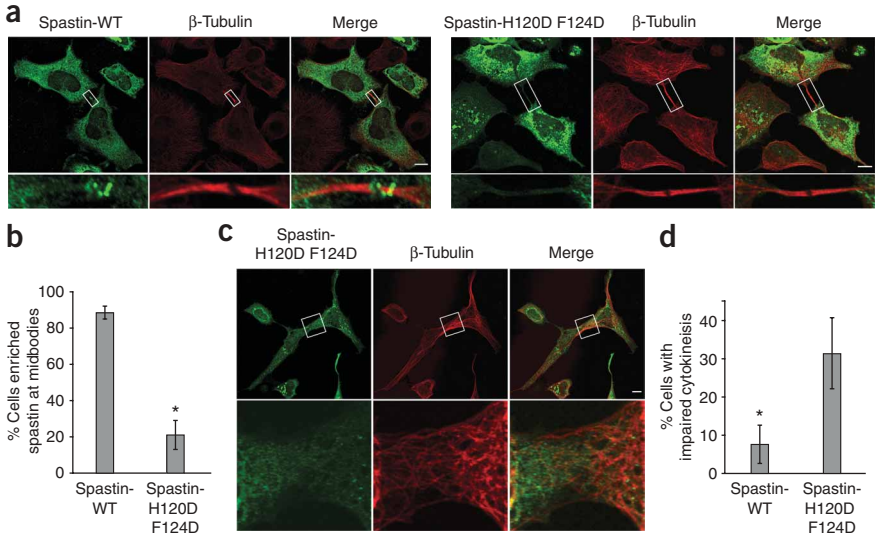

Figure 5 The Spastin MIT domain mutant protein shows decreased enrichment at midbodies and alters cytokinesis. (**a**) HeLa cells expressing wild-type (WT) Myc-spastin (above, green) or Myc–spastin-H120D F124D (below, green) were co-immunostained for Myc epitope and β-tubulin. Myc–spastin-H120D F124D shows decreased enrichment at midbodies, as identified by β-tubulin. Boxed areas are enlarged below. Scale bar, 10 μm. (**b**) Quantification of enrichment of wild-type versus MIT mutant spastin–expressing cells ($n = 3$; 100 cells per experiment; ± s.d.). * indicates $P = 0.001$. (**c**) HeLa cells expressing Myc–spastin-H120D F124D (green) showed impaired cytokinesis, with microtubules (red) often maintaining a connection between cells. The boxed area is enlarged below. Scale bar, 10 μm. (**d**) Quantification of cytokinesis impairment, as defined by the persistence of cellular interconnections, in wild-type Myc-spastin versus Myc–spastin-H120D F124D–expressing cells ($n = 3$; 100 cells per experiment; ± s.d.). * indicates $P < 0.05$.

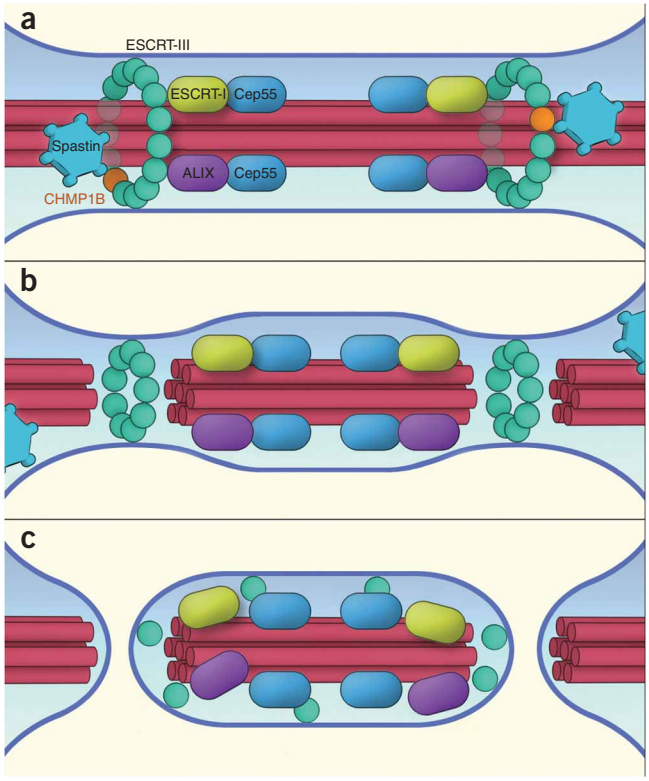

Figure 6 Speculative model for the role of the spastin–ESCRT-III interaction in cytokinesis. (**a**) The assembly of CEP55, ESCRT-I and ALIX at the midbody is postulated to recruit ESCRT-III (green spheres indicate generic ESCRT-III subunits). Coassembly of CHMP1B (orange sphere) into the ESCRT-III array leads to allosteric activation of CHMP1B, exposing its C-terminal helix, thereby leading to the recruitment of spastin (blue hexagon). The circular array of ESCRT-III proteins is depicted schematically as inspired by observations of their formation of spiral or helical arrays[10,11]. Two CEP55–ESCRT–spastin assemblies are shown in accordance with the double-cluster visible in **Figure 1a** and refs. 4,5,20. (**b**) Cleavage of the microtubules (red tubes) by spastin opens a path for ESCRT-III to sever the membrane neck. Direct proof that ESCRT-III severs membrane necks is lacking, but it is widely believed to have such an activity, perhaps in conjunction with other ESCRT components[2]. (**c**) Midbody resolution can occur on both sides leaving behind a free midbody fragment that is sometimes observed in cell culture, or it may occur stochastically on one side or the other.

DISCUSSION

The goal of this study was to explore the interaction between spastin and the ESCRT protein CHMP1B[16]. We replicated and extended a previously reported yeast two-hybrid analysis[16] and found that the MIT domain of spastin interacted robustly with CHMP1B, but with none of the other ten known human CHMP proteins. Furthermore, the interaction with the C-terminal CHMP1B fragment was stronger than the interaction with the full-length protein. This is consistent with the concept that monomeric full length ESCRT-III proteins are in an autoinhibited conformation in which the C-terminal helix folds back over the rest of the protein, blocking its access to potential binding partners[21–23]. Finally, the crystal structure of the complex indicates an interaction interface twice as large and a much more extensive involvement of hydrogen bonds than observed in other MIT domain–ESCRT-III complexes[14,15]. The predominance of hydrogen bonds in this complex is important, because these interactions have a directional dependence that demands exquisite specificity, in contrast to hydrophobic interactions. Furthermore, the functional importance of these interactions was validated by mutational analysis. These factors taken together pointed unequivocally to a highly specific interaction, one that is therefore likely to be physiologically relevant.

The structural results highlight the complexity of ESCRT recognition by MIT domains. The C-terminal helices of yeast Vps2 and Did2, and their respective human orthologs CHMP2 and CHMP1, contain (D/E/Q)xxLxx(Q/R)LxxL(K/R) sequences, now known as MIMs, that are responsible for binding to the Vps4 MIT domain[15]. However, MIT domains are a divergent family, and indeed many MIT domains are difficult to identify on the basis of sequence similarity in the absence of three-dimensional structures. For example, Vta1 contains two divergent MIT domains identified on the basis of its three-dimensional structure[24]. The second Vta1 MIT domain binds to Did2 and Vps60, the yeast ortholog of human CHMP5 (ref. 25). The human ortholog of Vta1 binds tightly to CHMP5 and also to CHMP1B, CHMP2A and CHMP3 (ref. 26). The MIT domains of AMSH and UBPY bind to distinct but overlapping subsets of ESCRT-III subunits[27–30], most of which do not contain the putative MIM consensus sequence. Although the spastin MIT domain is more closely related to that of VPS4 than some of the others mentioned above, structural analysis shows that it uses a completely different read-out mechanism from that used by VPS4. While this paper was under review, the structure of an extended motif from CHMP6 now designated 'MIM2' was determined in complex with the MIT domain of VPS4 (ref. 31) and shown to bind between helices 1 and 3, as seen also in the CHMP1B–spastin MIT complex. However, the CHMP6–MIM2 is extended in conformation, rather than helical, and the molecular contacts are not conserved between these complexes. It now seems that an elaborate recognition code embedded at distinct but overlapping sites in ESCRT-III C termini, as opposed to a single consensus sequence, is read out by a divergent collection of MIT domains. The high density of regulatory information packed into the C termini of ESCRT-III subunits is reminiscent of other biologically critical tail sequences, such as the N-terminal regions of histones.

The main biological finding in this study is that CHMP1B recruits spastin to the midbody, as knockdown of CHMP1B results in a diminution of Myc-tagged spastin localization to midbodies. The observation that some spastin remains at midbodies in these cells might be indicative of multiple interactions between spastin and other midbody proteins such as NA14 (ref. 19), the presence of residual CHMP1B in some cells owing to incomplete knockdown, or both. Because the reduction in spastin localization at midbodies was not complete, it is not surprising that cytokinesis was not markedly impaired in the CHMP1B knockdown cells (see also the **Supplementary Discussion** online). The finding that CHMP5 knockdown did not have a substantial effect on spastin recruitment suggests that spastin recruitment results from a specific action of CHMP1B rather than a generic role of CHMP1B in midbody morphology.

In an effort to resolve the functional role of the CHMP1B–spastin interaction in recruitment more definitively, we engineered a spastin mutant with an inactivated CHMP1B binding site. We selected the double mutation H120D F124D on the basis of the crystal structure, *in vitro* binding analysis and yeast two-hybrid studies. This site was chosen to engineer a selective knockout of CHMP1B binding because of the extraordinarily high specificity of this binding site. In contrast to wild-type spastin, we rarely observed the spastin-H120D F124D mutant at midbodies. The mutant was probably more effective than the CHMP1B siRNA knockdown at blocking midbody localization of spastin, because the mutations, even singly, are such potent disruptors of CHMP1B binding.

Expression of spastin-H120D F124D introduced a cytokinesis defect, whereas no such effect was observed upon expression of wild-type spastin. Spastin functions as a hexamer and is presumably targeted to midbodies through high-avidity interactions with oligomeric CHMP1B. We speculate that the the overexpressed spastin-H120D F124D mutant acts in a dominant negative manner, inactivating endogenous spastin, which is diluted into hexamers consisting primarily of mutant monomers incapable of binding CHMP1B. The localization of spastin to the midbody via the ESCRTs, and the observed defect in cytokinesis, suggest to us that spastin has a role in cytokinesis. Given the centrality of microtubules in cell division, the possibility that a microtubule-severing enzyme has such a role should not be surprising. In a reasonable working model incorporating the results reported here and those of others, CEP55 recruits ALIX and ESCRT-I[4,5], which recruit the ESCRT-III subunits CHMP4 (ref. 20) and CHMP6, respectively. CHMP4 and CHMP6 recruit CHMP2 and CHMP3, which in turn recruit CHMP1 and CHMP5 (ref. 2), and finally, through CHMP1B, spastin. These results suggest that microtubule severing and membrane abscission could be coordinated through the spastin–ESCRT connection (**Fig. 6**). The precise mechanistic basis for the cytokinesis defect, and its relationship to other cellular functions of spastin, will be an important topic for further analysis.

METHODS

DNA constructs. The human spastin (GenBank NM_014946) coding sequence was cloned into the EcoRI site of the mammalian expression vector pGW1-Myc, which contains an N-terminal Myc-epitope tag[32]. The second ATG start codon at amino acid position 88 was used for all recombinant expression studies[33]. Human CHMP1B (GenBank NM_020412) was cloned into the EcoRI site of the mammalian expression vector pGW1-HA, which contains an N-terminal hemagglutinin (HA)-epitope tag[32]. EcoRI fragments comprising spastin residues 110–195 and VPS4A (GenBank NM_013245) residues 1–82 were cloned into pBHA and pGBKT7 yeast two-hybrid bait vectors, respectively. The full coding sequences and indicated deletion constructs for CHMP1A (GenBank NM_002768), CHMP1B, CHMP2A (GenBank NM_014453), CHMP4A (GenBank NM_014169), CHMP4B (GenBank NM_176812), CHMP4C (GenBank NM_152284), CHMP5 (GenBank NM_016410), CHMP6 (GenBank NM_024591) and CHMP7 (GenBank NM_152272) were cloned into the EcoRI or EcoRI/XhoI sites of the yeast two-hybrid prey vector pGAD10. CHMP3 (GenBank NM_001005753) and CHMP2B (GenBank NM_014043) were cloned into the XmaI site of pGADT7. Site-directed mutagenesis was performed using QuikChange (Stratagene).

Antibodies. Mouse monoclonal antibodies were used against β-tubulin (IgG_1, clone D66; Sigma-Aldrich), and PLCγ (Upstate Biotechnology). Rabbit polyclonal antibodies were used against β-tubulin and hemagglutinin epitope (Abcam). Mouse polyclonal Anti-CHMP1B anti-CEP55 antibodies were obtained from Abnova. Goat polyclonal anti–Myc epitope antibodies were obtained from Bethyl Laboratories, and goat polyclonal anti-CHMP5 antibodies from Abcam. Alexa Fluor secondary antibodies were obtained from Invitrogen.

Cell culture and transfection. HeLa cells were maintained in DMEM with 10% (v/v) FBS, plated on coverslips in six-well plates, and transfected with 1 μg of plasmid DNA using Lipofectamine (Invitrogen). After 24 h, cells were washed in PBS, pH 7.4, and fixed using methanol. Cells used for immunoblot analysis were washed with PBS and collected in 0.1% (w/v) Triton X-100 in PBS. For siRNA transfections, HeLa cells were plated at 50% confluency and transfected the next morning with 100 nM siRNA oligonucleotides using Oligofectamine (Invitrogen) for 4 h. Cells were scraped for immunoblot analysis or fixed for immunocytochemical analysis 72 h after transfection. CHMP1B-specific siRNA oligonucleotides (Invitrogen) were as follows: 1, 5′-GGGCAACAUG GAAGUUGCGAGGAUA-3′; #2, 5′-GAAGACACGAUGAGCAGCACGACGA-3′; #3, 5′-UCGACCUCAACAUGGAGCUGCCGCA-3′. The CHMP5-specific siRNA nucleotide (Invitrogen) was 5′-GGUGGACAGUAGAGCAGAAUCCAUU-3′.

Table 1 Data collection, phasing and refinement statistics

		SeMet		
Data collection				
Space group		$P2_12_12$		
Cell dimensions				
a, *b*, *c* (Å)		151.97, 95.49, 100.36		
		Peak	*Inflection*	*Remote*
Wavelength		0.9792	0.9793	0.9717
Resolution (Å)		2.5	2.5	2.5
R_{sym}		10.0 (41.4)	11.2 (43.6)	10.1 (46.6)
$I / \sigma I$		28.3 (4.0)	29.4 (4.0)	26.2 (3.4)
Completeness (%)		98.1 (85.8)	98.3 (87.3)	97.1 (79.8)
Redundancy		9.2 (7.1)	9.6 (7.0)	9.2 (6.9)
Refinement				
Resolution (Å)	2.5			
No. reflections	48,059			
R_{work} / R_{free}	23.2/26.8			
No. atoms				
Protein	5,985			
B-factor				
Protein	53.7			
r.m.s. deviations				
Bond lengths (Å)	0.013			
Bond angles (°)	1.1			
Ramachandran plot				
Most favored regions	95.7%			
Additional allowed regions	3.7%			
Generously allowed regions	0.6%			
Disallowed regions	0.0%			

A single SeMet crystal was used for both structure determination at 3.0-Å resolution and refinement (inflection point data set). Values in parentheses are for the highest-resolution shell.

Confocal microscopy. Cells were imaged using a Zeiss LSM510 confocal microscope with a 63× 1.4 NA Plan-APOCHROMAT lens. Acquisition was performed using LSM 510 version 3.2 SP2 software (Carl Zeiss Microimaging). Data were processed using Adobe Photoshop 7.0 and Adobe Illustrator CS2 software. For quantification studies, at least 100 cells were counted per experimental group, and experiments were conducted at least three times. Spastin enrichment at midbodies was quantified by assessing all Myc-spastin–transfected cells with a midbody present. To quantify 'impaired cytokinesis', every pair of adjacent transfected cells was assessed for whether the cells were still interconnected. Statistical significance was assessed using two-tailed, unpaired Student's *t*-tests, assuming unequal variance.

Yeast two hybrid analysis. Yeast two-hybrid tests using AH109 and L40 yeast strains were performed as described previously[32].

Protein cloning, expression and purification. The human spastin MIT domain (residues 112–195) and the CHMP1B C-terminal region (residues 126–199; CHMP1B-CTR) were cloned into pHis2 vector and expressed in Rosetta (DE3) cells. For MAD phasing, SeMet-substituted CHMP1B-CTR was expressed in B834(DE3) cells using autoinduction[34]. Cells were lysed in buffer A (20 mM Tris, 500 mM NaCl, 20 mM imidazole and 10% (v/v) glycerol, pH 8.0) using sonication. Cell lysates were applied to a HisTrap HP column (GE Healthcare). The spastin MIT domain was eluted under 20 mM Tris, 500 mM

NaCl, 10% (v/v) glycerol and a gradient of 60–250 mM imidazole, pH 8.0. CHMP1B-CTR was eluted with the same buffer and a gradient of 60–120 mM imidazole, pH 8.0. The eluted protein was dialyzed in 20 mM Tris and 100 mM NaCl, pH 8.0 (for SeMet CHMP1B-CTR and the MIT domain, the buffer also contained 14 mM β-mercaptoethanol). The His_6-tag was removed by cleavage with TEV protease (100:1 (w/w)) at room temperature for 16 h, and the cleaved protein was separated from the TEV protease and uncleaved material by passage through a HisTrap HP column. The purified MIT domain and CHMP1B-CTR terminus were mixed at a 1:1 molar ratio, incubated at 4 °C for 16 h, concentrated and then applied to Superdex 75 size-exclusion column. The MIT–CHMP1B-CTR complex was eluted using 20 mM Tris, 100 mM NaCl and 14 mM β-mercaptoethanol, pH 8.0.

GST pull-down experiments. Cultures (100 ml) of *Escherichia coli* expressing GST, GST-CHMP1A (123–196) and GST-CHMP1B (126–199) were harvested, resuspended in 10 mM Tris, 250 mM NaCl, 10 mM imidazole and 5% (v/v) glycerol, and lysed by sonication. After centrifugation, the lysate was incubated with 500 µl glutathione agarose slurry (GE Healthcare) in a total volume of 50 ml at 4 °C overnight. The agarose was collected by centrifugation at 600*g* and washed with 50 ml PBS buffer three times. Pull-down reactions were performed by incubating 30 µl glutathione agarose that already had GST, GST-CHMP1A (123–196) or GST-CHMP1B (126–199) bound with the addition of 10 µl of spastin MIT protein at 10 mg ml^{-1} concentration). Binding was performed at 4 °C for 2 h, and the agarose was collected by centrifugation at 600*g* and washed three times with 1 ml PBS. Bound and unbound samples were then analyzed by SDS-PAGE. The competition assay in **Figure 4f** was performed by mixing 30 µl of glutathione resin bound with GST or GST–CHMP1B-CTR, 70 µl of 140 µM His_6–VPS4 MIT (except for lane 7) and 0–100 µl of 960 µM spastin MIT. The total reaction volume was then brought up to 800 µl by PBS buffer. After incubating at 4 °C for 2 h, the resin was washed and the results analyzed by SDS-PAGE in the same way as described for the GST pull-down experiments. To test whether the CHMP1B-L188A L192A mutant bound MIT domains (**Supplementary Fig. 7**), 30 µl of glutathione resin bound with GST or GST–CHMP1B-CTR (wild type or mutant) was mixed with 70 µl of 140 µM His_6–VPS4 MIT or 10 µl of 960 µM spastin MIT. The total reaction volume was adjusted to 100 µl using PBS. Subsequent experimental steps were identical to those described earlier.

Surface plasmon resonance. Binding of the spastin MIT domain to CHMP1B-CTR was analyzed using a Biacore T100 instrument at 25 °C with a flow rate of 10 µl min^{-1}. Wild-type or mutant His_6-tagged CHMP1B-CTR samples were diluted to 20 µM in 10 mM acetate buffer, pH 4.0, and immobilized by passage over a CM5 chip that had been activated by a 1:1 mixture of N-hydroxysuccinimide (NHS) and 1-ethyl-3-(3-dimethylaminopropyl)carbodiimide (EDC) at a flow rate of 10 µl min^{-1}. After the immobilization step, the CM5 surface was blocked by 1 M ethanolamine at pH 8.5. Binding studies were performed by passing the spastin and VPS4A MIT domains over the immobilized CHMP1B-CTR at a flow rate of 10 µl min^{-1}. The association and dissociation times were 180 s and 100 s, respectively. The surface was regenerated with an injection of 10 mM glycine-HCl, pH 2.2, at a flow rate of 10 µl min^{-1} for 30 s.
The data were fit with the following equation:

$$R = R_{max}[MIT]/(K_d + [MIT]) + offset$$

where [MIT] is the protein concentration of the flowing analyte, K_d is the dissociation constant, R_{max} is the maximal response, and 'offset' is the background signal. The data were fit using BiaEvaluation (Biacore) and GraphPad Prism software (GraphPad Software).

Crystallization. Crystals of the spastin MIT domain with the CHMP1B-CTR were produced by the hanging drop vapor diffusion method from a 1:1 mixture of protein solution at 40–60 mg ml^{-1} protein, with a reservoir solution containing 10% (v/v) PEG2000 MME, 0.2 M $(NH_4)_2SO_4$ and 0.1 M sodium acetate, pH 4.6. For data collection, 25% (v/v) glycerol was used as a cryoprotectant and crystals were frozen by immersion in liquid nitrogen.

Structure determination. A native spastin MIT domain–SeMet CHMP1B-CTR cocrystal was used to collect a MAD data set at 100 K at beamline 22-ID, Advanced Photon Source (**Table 1**). Initial phases were calculated at 3.0 Å using SOLVE[35] and an interpretable electron density map was generated using RESOLVE[36]. Automatic model building in RESOLVE covered roughly 75% of the residues, and model building was then completed manually using COOT[37]. There are six complexes within each asymmetric unit. Thin resolution shells of test reflections were used for validation during refinement. The model was refined using simulated annealing with CNS[38] and restrained refinement in REFMAC[39].

Accession codes. Protein Data Bank: Crystallographic coordinates for the spastin MIT–CHMP1B-CTR complex have been deposited with accession code 3EAB.

Note: Supplementary information is available on the Nature Structural & Molecular Biology website.

ACKNOWLEDGMENTS

We thank N. Elia for discussions, the staff of SER-CAT for user support at the Advance Photon Source (APS), C.-R. Chang for technical assistance, E. Tyler for generating **Figure 6** and D. Davies for comments on the manuscript. Use of the APS was supported by the US Department of Energy, Basic Energy Sciences, Office of Science, under Contract No.W-31-109-Eng-38. This project was funded by the Intramural Research Programs of US National Institute of Diabetes and Digestive and Kidney Diseases, US National Institute of Neurological Disorders and Stroke and the US National Institute of Child Health and Human Development, and the Bench-to-Bedside program of the US National Institutes of Health (NIH).

AUTHOR CONTRIBUTIONS

D.Y. carried out binding experiments, crystallization and structure determination; N.R. and B.R. carried out knockdown and cell-imaging experiments; J.L.-S. interpreted data; C.B. carried out yeast two-hybrid experiments; C.B. and J.H.H. designed research, interpreted data and wrote the paper.

Published online at http://www.nature.com/nsmb/
Reprints and permissions information is available online at http://npg.nature.com/reprintsandpermissions/

1. Saksena, S., Sun, J., Chu, T. & Emr, S.D. ESCRTing proteins in the endocytic pathway. *Trends Biochem. Sci.* **32**, 561–573 (2007).
2. Hurley, J.H. ESCRT complexes and the biogenesis of multivesicular bodies. *Curr. Opin. Cell Biol.* **20**, 4–11 (2008).
3. Morita, E. & Sundquist, W.I. Retrovirus budding. *Annu. Rev. Cell Dev. Biol.* **20**, 395–425 (2004).
4. Carlton, J.G. & Martin-Serrano, J. Parallels between cytokinesis and retroviral budding: a role for the ESCRT machinery. *Science* **316**, 1908–1912 (2007).
5. Morita, E. *et al.* Human ESCRT and ALIX proteins interact with proteins of the midbody and function in cytokinesis. *EMBO J.* **26**, 4215–4227 (2007).
6. Glotzer, M. The molecular requirements for cytokinesis. *Science* **307**, 1735–1739 (2005).
7. Skop, A.R., Liu, H.B., Yates, J., Meyer, B.J. & Heald, R. Dissection of the mammalian midbody proteome reveals conserved cytokinesis mechanisms. *Science* **305**, 61–66 (2004).
8. Gromley, A. *et al.* Centriolin anchoring of exocyst and SNARE complexes at the midbody is required for secretory-vesicle-mediated abscission. *Cell* **123**, 75–87 (2005).
9. Pohl, C. & Jentsch, S. Final stages of cytokinesis and midbody ring formation are controlled by BRUCE. *Cell* **132**, 832–845 (2008).
10. Hanson, P.I., Roth, R., Lin, Y. & Heuser, J.E. Plasma membrane deformation by circular arrays of ESCRT-III protein filaments. *J. Cell Biol.* **180**, 389–402 (2008).
11. Lata, S. *et al.* Helical structures of ESCRT-III are disassembled by VPS4. *Science* **321**, 1354–1357 (2008).
12. Dukes, J.D., Richardson, J.D., Simmons, R. & Whitley, P. A dominant-negative ESCRT-III protein perturbs cytokinesis and trafficking to lysosomes. *Biochem. J.* **411**, 233–239 (2008).
13. Hurley, J.H. & Yang, D. MIT domainia. *Dev. Cell* **14**, 6–8 (2008).
14. Stuchell-Brereton, M.D. *et al.* ESCRT-III recognition by VPS4 ATPases. *Nature* **449**, 740–744 (2007).
15. Obita, T. *et al.* Structural basis for selective recognition of ESCRT-III by the AAA ATPase Vps4. *Nature* **449**, 735–739 (2007).
16. Reid, E. *et al.* The hereditary spastic paraplegia protein spastin interacts with the ESCRT-III complex-associated endosomal protein CHMP1B. *Hum. Mol. Genet.* **14**, 19–38 (2005).
17. Soderblom, C. & Blackstone, C. Traffic accidents: molecular genetic insights into the pathogenesis of the hereditary spastic paraplegias. *Pharmacol. Ther.* **109**, 42–56 (2006).

18. Roll-Mecak, A. & Vale, R.D. Structural basis of microtubule severing by the hereditary spastic paraplegia protein spastin. *Nature* **451**, 363–367 (2008).
19. Errico, A., Claudiani, P., D'Addio, M. & Rugarli, E.I. Spastin interacts with the centrosomal protein NA14, and is enriched in the spindle pole, the midbody and the distal axon. *Hum. Mol. Genet.* **13**, 2121–2132 (2004).
20. Carlton, J.G., Agromayor, M. & Martin-Serrano, J. Differential requirements for Alix and ESCRT-III in cytokinesis and HIV-1 release. *Proc. Natl. Acad. Sci. USA* **105**, 10541–10546 (2008).
21. Zamborlini, A. *et al.* Release of autoinhibition converts ESCRT-III components into potent inhibitors of HIV-1 budding. *Proc. Natl. Acad. Sci. USA* **103**, 19140–19145 (2006).
22. Shim, S., Kimpler, L.A. & Hanson, P.I. Structure/function analysis of four core ESCRT-III proteins reveals common regulatory role for extreme C-terminal domain. *Traffic* **8**, 1068–1079 (2007).
23. Lata, S. *et al.* Structural basis for autoinhibition of ESCRT-III CHMP3. *J. Mol. Biol.* **378**, 818–825 (2008).
24. Xiao, J. *et al.* Structural basis of Vta1 function in the multi-vesicular body sorting pathway. *Dev. Cell* **14**, 37–49 (2008).
25. Azmi, I.F. *et al.* ESCRT-III family members stimulate Vps4 ATPase activity directly or via Vta1. *Dev. Cell* **14**, 50–61 (2008).
26. Shim, S., Merrill, S.A. & Hanson, P.I. Novel interactions of ESCRT-III with LIP5 and VPS4 and their implications for ESCRT-III disassembly. *Mol. Biol. Cell* **19**, 2661–2672 (2008).
27. Tsang, H.T.H. *et al.* A systematic analysis of human CHMP protein interactions: additional MIT domain-containing proteins bind to multiple components of the human ESCRT III complex. *Genomics* **88**, 333–346 (2006).
28. Agromayor, M. & Martin-Serrano, J. Interaction of AMSH with ESCRT-III and deubiquitination of endosomal cargo. *J. Biol. Chem.* **281**, 23083–23091 (2006).
29. Ma, Y.M. *et al.* Targeting of AMSH to endosomes is required for epidermal growth factor degradation. *J. Biol. Chem.* **282**, 9805–9812 (2007).
30. Row, P.E. *et al.* The MIT domain of UBPY constitutes a CHMP binding and endosomal localization signal required for efficient EGF receptor degradation. *J. Biol. Chem.* **282**, 30929–30937 (2007).
31. Kieffer, C. *et al.* Two distinct modes of ESCRT-III recognition are required for VPS4 functions in lysosomal protein targeting and HIV-1 budding. *Dev. Cell* **15**, 62–73 (2008).
32. Blackstone, C., Roberts, R.G., Seeburg, D.P. & Sheng, M. Interaction of the deafness-dystonia protein DDP/TIMM8a with the signal transduction adaptor molecule STAM1. *Biochem. Biophys. Res. Commun.* **305**, 345–352 (2003).
33. Yu, W. *et al.* The microtubule-severing proteins spastin and katanin participate differently in the formation of axonal branches. *Mol. Biol. Cell* **19**, 1485–1498 (2008).
34. Studier, F.W. Protein production by auto-induction in high-density shaking cultures. *Protein Expr. Purif.* **41**, 207–234 (2005).
35. Terwilliger, T.C. & Berendzen, J. Automated MAD and MIR structure solution. *Acta Crystallogr. D Biol. Crystallogr.* **55**, 849–861 (1999).
36. Terwilliger, T.C. Maximum-likelihood density modification. *Acta Crystallogr. D Biol. Crystallogr.* **56**, 965–972 (2000).
37. Emsley, P. & Cowtan, K. Coot: model-building tools for molecular graphics. *Acta Crystallogr. D Biol. Crystallogr.* **60**, 2126–2132 (2004).
38. Brunger, A.T. *et al.* Crystallography & NMR system: a new software suite for macromolecular structure determination. *Acta Crystallogr. D Biol. Crystallogr.* **54**, 905–921 (1998).
39. Murshudov, G.N., Vagin, A.A. & Dodson, E.J. Refinement of macromolecular structures by the maximum- likelihood method. *Acta Crystallogr. D Biol. Crystallogr.* **53**, 240–255 (1997).